Received: 22 August 2024 | Revised: 26 September 2024 | Accepted: 27 October 2024

DOI: 10.1002/efd2.70020

RESEARCH ARTICLE

eFood WILEY

Effect of *Mesembryanthemum crystallinum* and its derived D-pinitol on HMG-CoA reductase and tyloxapol-induced hyperlipedemia

Jun-Hui Choi | **Se-Eun Park** | **Seung Kim**

Department of Health Functional Food, Gwangju University, Gwangju, Republic of Korea

Correspondence

Seung Kim, Department of Health Functional Food, Gwangju University, Gwangju 61743, Republic of Korea.
Email: seungk@gwangju.ac.kr

Funding information

Ministry of SMEs and Startups, Grant/Award Number: RS-2023-00224984

Abstract

Several previous research indicate that treating *Mesembryanthemum crystallinum* may aid in reducing adipogenesis and triacylglycerol level and improving hyperglycemia and diabetes. Therefore, the present study was designed to evaluate the effectiveness of *M. crystallinum* extract (MCE) in combating obesity and lowering fat/lipid/cholesterol levels. The study aimed to investigate the molecular docking model targeting 3-hydroxy-3-methylglutaryl-CoA reductase (HMGCR) using MCE-derived D-pinitol or atorvastatin, an inhibitor of HMGCR. In this study, histological alterations in the liver of tyloxapol-induced hyperlipidemia (TIH) model, hyperlipidemia-related markers in serum, HMGCR activity, and cell viability in HepG2 cells were analyzed. Our findings revealed that tyloxapol treatment significantly led to increased hyperlipidemia-related indicators and cardiovascular-associated risk indices. However, MCE effectively mitigated tyloxapol-induced hepatic fat accumulation and an increase in cholesterol levels. This was achieved through improvements in metabolic parameters, ultimately ameliorating TIH. These beneficial results suggest that MCE may be a strong potential for the treatment of hyperlipidemia-related diseases.

KEYWORDS

anti-hyperlipidemia, D-pinitol, hyperlipidemia, *Mesembryanthemum crystallinum*

1 | INTRODUCTION

Elevated cholesterol levels are linked to numerous diseases, particularly coronary heart disease, encompassing conditions such as ischemic stroke, atherosclerosis, hypertension, diabetes, myocardial infarction, and coronary artery disease. Unregulated cholesterol consumption plays a pivotal role in foam cell formation and atherogenesis. Increased levels of low-density lipoprotein (LDL) heighten an individual's susceptibility to atherosclerosis and its complications, correlating with cardiovascular risk in human populations (Saxena & Chandra, 2020). The correlation between a high concentration of high-density lipoprotein (HDL) cholesterol or a low concentration of LDL and a reduced risk of atherosclerotic cardiovascular disease is widely acknowledged (Palabıyık et al., 2023). Fenofibrate, used to treat hyperlipidemia (Canzler & Bojanovski, 1980), is known to reduce lipoprotein levels in ob/ob mice (Zhang et al., 2022) or hyperlipidemic mice (Olivier et al., 1988), and in addition, numerous studies have explored methods including intracellular triglyceride/cholesterol lowering (Lee et al., 2019), fat accumulation reducing effect (Choi et al., 2020; Mo), reducing blood triglyceride (TG) (Mozaffarian et al., 2022), modulating metabolic enzymes activity (Palabıyık et al., 2023; Sulumer et al., 2024) using natural or food materials, and lipid-reducing antioxidant compounds (Ramos et al., 2021) to decrease LDL levels and elevate HDL concentrations. Fat accumulation in the liver promotes the synthesis of neutral fat, which in turn triggers the secretion of very LDL, contributing to insulin resistance

This is an open access article under the terms of the Creative Commons Attribution License, which permits use, distribution and reproduction in any medium, provided the original work is properly cited.
© 2024 The Author(s). *eFood* published by John Wiley & Sons Australia, Ltd on behalf of International Association of Dietetic Nutrition and Safety.

in the liver. Furthermore, obesity and related metabolic disease resulting from fat buildup elevate the risk of developing conditions such as hyperlipidemia, high blood pressure, coronary cardiovascular disease, arthritis, gallbladder disease, and specific cancers (Palabıyık et al., 2023). As one of the most abundant free fatty acids in a high-lipid diet, palmitic acid exposure results in intracellular lipid accumulation in hepatocytes by activating sterol regulatory element-binding protein (SREBP) and 3-hydroxy-3-methylglutaryl-CoA reductase (HMGCR) (Lu et al., 2019). The enzyme HMGCR, which initiates cholesterol biosynthesis from acetate, serves as a therapeutic target for hyperlipidemia (Kim et al., 2023). Upon cholesterol transportation from the intestine to the liver, inhibition of HMGCR, the enzyme responsible for converting HMG-CoA to mevalonate in cholesterol synthesis, results in decreased production of endogenous cholesterol by the liver (Han et al., 2014). Various inhibitors of HMGCR, such as statin, atorvastatin, simvastatin, and pitavastatin have been developed for the treatment of hyperlipidemia (Guan et al., 2008; Han et al., 2014; Hu et al., 2021; Kumai et al., 2004).

Ice plant, scientifically known as *Mesembryanthemum crystallinum*, belongs to the Aizoaceae family and its moniker "ice plant" stems from the striking resemblance of its stems and leaves to ice crystals. Utilized in traditional medicine and high-functional food, its leaves and stems are employed in treating liver and kidney ailments and the plant contains polyol, which confers antioxidant properties (Agarie et al., 2009; Ibtissem et al., 2012). Recognized in Japan and Europe for its efficacy in preventing adult-onset diseases, lung inflammation, and painful urination, it is esteemed as a highly functional botanical resource (Foster & Hobbs, 2002; Kang et al., 2016). Ice plant bladder cells, resembling ice crystals on the stems and leaves, harbor beneficial components for human health, including various minerals, beta-carotene, and inositol. The *M. crystallinum* extract (MCE) is a valuable source of D-pinitol, known to regulate blood sugar levels, recognized for its ability to inhibit triglyceride level (Drira et al., 2016), and its potential antidiabetic properties (Zhang et al., 2019) and regarded as the contributor behind the ice plant's anti-hyperlipidemic properties. Therefore, the present study was designed to analyze the D-pinitol content of the ice plant *M. crystallinum*, to evaluate the anti-hyperlipidemic effects or inhibitory effect against HMGCR of MCE and its derived D-pinitol, and to compare the efficacy of MCE and fenofbrate in tyloxapol-induced hyperlipedemic mice model.

2 | MATERIALS AND METHODS

2.1 | Materials

Triton WR-1339, D-pinitol, Trizma base, fenofibrate, dimethyl sulfoxide (DMSO), ethylenediaminetetraacetic acid (EDTA), and Oil-Red O were purchased from Sigma-Aldrich. Dulbecco's modified Eagle's medium (DMEM), fetal bovine serum (FBS), streptomycin, and penicillin were purchased from Invitrogen. Other reagents were commercially available and of special grade.

2.2 | Extraction

Fresh *M. crystallinum* was obtained from the Nadeulmok farm in Yangnam-myeon, Gyeongju-si, Gyeongsangbuk-do, Republic of Korea in July 2023. The authenticity of the samples was confirmed by Professor Myung-Kon Kim from the Department of Food Science and Technology at Jeonbuk National University. According to the previously described method with a slight modification (Choi, Kim, Park, et al., 2023), the samples were washed with distilled water and then subjected to freeze-drying for 3 days. After that, the samples were ground into a powder using a household grinder and stored in airtight plastic bags in a freezer at –20°C. To prepare the MCE, 10 g of frozen powder was mixed with 30 mL of 100% ethanol aqueous solution and ultrasonicated at room temperature for 20 min. The mixture was then centrifuged at 4500 rpm for 10 min, and the resulting supernatant was collected. This process was repeated twice, and the collected supernatants were concentrated and vacuum evaporated at 40°C. The resulting concentrated sample was dissolved in 30 mL of 50% ethanol, which was then shaken and ultrasonicated at room temperature for 20 min, and then centrifuged at 4000 rpm and 4°C. Finally, the concentrated sample was dissolved in 2 mL of ethanol, filtered using a microsyringe filter with a pore size of 0.45 μm, and used for high performance liquid chromatography (HPLC) analysis.

2.3 | HPLC analysis

HPLC analysis was performed using an HPLC system (Waters) equipped with a 2690 separation module and Waters RI with a NH2P-50 column (4.6 mm id × 250 mm, Shodex). For analysis of D-pinitol, the mobile phase comprised 25% water (solvent A) and 75% acetonitrile (solvent B) for 20 min at a flow rate of 1.0 mL/min. The injection volume was 10 μL and the oven temperature was set at 60°C. The quantification of D-pinitol was based on peak areas. The compound standard of D-pinitol was used for calibration curves. The standard solutions (175, 350, 700, 1400, and 2800 μg/mL) were prepared in 50% ethanol. The D-pinitol compound from MCE was identified based on the retention time of the standard and quantified by comparing the peak area intensity with the standard curve.

2.4 | Cell culture

HepG2 cells sourced from the Korean Cell Line Bank were utilized in the study as previously described (Choi

et al., 2020). DMEM added with 1% streptomycin-penicillin and 10% FBS was employed for cell culture, maintained at 37°C with 5% CO_2. Upon reaching approximately 80% confluency, HepG2 cells were sub-cultured and subjected to serum-free DMEM for 24 h before treatment with 50, 100, 300, 500, 700, 900, and 1000 μM palmitic acid and MCE for another 24 h. The control group received treatment involving the addition of 5% bovine serum albumin to the medium.

2.5 | Preparation of palmitic acid solution

The preparation of the palmitic acid solution followed a modification of the method outlined by Cousin et al. (2001). Initially, a 100 mM palmitic acid stock solution was created by heating in a 0.1 mM NaOH solution at 70°C. Subsequently, a 10 mM FFA/1% BSA solution was generated by combining the palmitic acid stock solution with a 10% (w/v) FFA-free BSA solution held at 55°C in ddH_2O, and allowed to react for 30 min. Afterward, the resultant solution was cooled to 25°C, filtered, stored at –20°C, and utilized in the experiment.

2.6 | Cell viability assay

HepG2 cells were seeded in a plate with 96-well at a density of 4×10^4 cells per well, then subjected to treatment with palmitic acid and MCE, and cultured for 24 h as previously described (Choi & Kim, 2018). Following the incubation period, the medium was aspirated, and 10 μL of a 5 mg/mL of 3-(4,5-dimethylthiazol-2-yl)-2,5-diphenyl tetrazolium bromide (MTT) solution was treated, allowing for a 4-h reaction. Upon completion of the reaction, the resultant formazan crystals in each well were dissolved using 100 μL of DMSO, and the absorbance was assessed at 540 nm using an ELISA reader.

2.7 | HMGCR activity analysis

Since palmitic acid, is one of the most abundant free fatty acids in the high lipid diet, exposure leads to intracellular lipid accumulation in hepatocytes by activating SREBP and HMGCR (Lu et al., 2019), its effect on HMGCR activation and inhibitory effect of MCE were examined. HepG2 cells were treated with MCE or atorvastatin, and palmitic acid in a six-well plate for 16 h. After treatment, the cell medium was removed and washed with phosphate buffered saline (PBS, Welgene). The washed cells were lysed using lysis buffer (150 mM NaCl, 0.1% SDS, 1% sodium deoxycholate, 2 mM EDTA, 1% Triton X-100, 10 mM phosphate buffer pH 7.4), centrifuged at 12,000 rpm for 10 min, and the supernatant was separated and used for HMGCR activity analysis. HMGCR activity was confirmed by performing the analysis according to the analysis method provided by the manufacturer using the HMGCR activity assay kit (Sigma-Aldrich) (Lee et al., 2019).

2.8 | Molecular docking

Molecular docking analysis utilized Human HMGCR (PDB code: 1HWK), along with D-pinitol (PubChem CID: 164619), and atorvastatin (PubChem CID: 60823). AutoDock4 (Morris et al., 2009) and PyMol (Schrodinger, 2010) facilitated the analysis process as previously described (Choi, Park, et al., 2023). AutoDock Vina software was employed to predict the binding energy scores between the experimental ligands (D-pinitol, and atorvastatin) acting as inhibitors and the protein HMGCR. AutoDock Vina, designed specifically for protein–ligand docking, is a molecular modeling and simulation software (Choi, Park, et al., 2023). For molecular binding analysis, grid maps encompassing all residues were generated, with the number of evaluations set at 2,500,000 and the number of runs at 10. The docking outcomes were computed using the Lamarckian Genetic Algorithm and visualized through AutoDockTools 1.5.6 and PyMol 3.0.0. AutoDockTools molecular graphics software facilitated modeling the complex structure of experimental ligands (D-pinitol, or atorvastatin) and HMGCR proteins via molecular docking across all amino acid residues within specific distances (Å). Utilizing Discovery Studio Visualizer 2021 software (Accelrys Software Inc.), images depicting enzyme binding pockets and binding profiles with ligands were generated.

2.9 | Toxicity predictions

To search the toxicity of MCE-derived compound, the ProTox 3.0 tool was used, which computes the prediction for acute toxicity, binding to 16 toxicity targets, and LD_{50} values (Banerjee et al., 2024).

2.10 | Animals

For the experiment on hyperlipidemic mice model, male imprinting control region (ICR) mice aged 10 weeks and weighing between 30 and 40 g were utilized. These mice were housed in cages accommodating three animals each and were maintained under controlled environmental conditions, with a 12-h light or dark cycle and a temperature range of 22 ± 2°C. The mice had unrestricted access to either standard feed (LabDiet 5L79; ORIENT BIO Inc.), as well as tap water ad libitum. The compositions of the administered diets are presented in Table 1. To alleviate animal distress and minimize the usage of animals, all experimental protocols adhered to the guidelines outlined in the National Institutes of Health Guide for the Care and Use of Laboratory Animals

TABLE 1 Composition of the experimental diets.

	w/w				
Composition	**Control**	**Model**	**Fenofibrate**	**MCE500**	**MCE1000**
Nitrogen-free extract	59.5	37.5	37.5	37.5	37.5
Fat	4.5	34.9	34.9	34.9	34.9
Protein	20.1	23.6	23.6	23.6	23.6
Fiber	4.6	-	-	-	-
Ash	5.8	-	-	-	-
Mineral mixture	3.5	3	3	3	3
Vitamin mixture	1	1	1	1	1
Fenofibrate	-	-	0.16	-	-
MCE	-	-	-	0.4	-
	-	-	-	-	0.8
Protein calories	21.0	18.1	18.1	18.1	18.1
Fat calories	13.7	61.6	61.6	61.6	61.6
Carbohydrates calories	65.3	20.3	20.3	20.3	20.3
Energy (kcal/g)	4.04	4.65	4.65	4.65	4.65

Note: The diets composition according to LabDiet 5L79 and TestDiet 58Y1. Fenofibrate, 200 mg/kg/day fenofibrate-administrated model group; MCE500-1000, 500, and 1000 mg/kg/day *Mesembryanthemum crystallinum* extract-administrated model group.

(NIH publication no. 80-23, revised 1996) and the relevant ethical regulations of Gwangju University. Furthermore, these experiments were approved by the Institutional Animal Care and Use Committee of Chosun University (CIACUC2023-S0032).

2.11 | In vivo hyperlipidemia mice model and treatment groups

The effect of MCE was investigated in hyperlipidemia mice. Tyloxapol (Triton WR-1339) was injected intraperitoneally in a dose of 300 mg/kg for hyperlipidemia model with elevation of triglycerides and cholesterols (Palabıyık et al., 2023), and MCE (1000 mg/kg/day), and fenofibrate (200 mg/kg/day) were orally treated for 50 days. The mice were divided into five groups, each consisting of six mice. Group 1 consisted of normal mice treated with saline as a vehicle and fed a standard diet (Control group). Group 2 comprised the hyperlipidemia mice model by intraperitoneal injection of tyloxapol and treated with saline as a vehicle tyloxapol-induced hyperlipidemia (TIH) (TIH group). Groups 3–5 included the TIH mice model treated with 500 mg/kg MCE (TIH+MCE500 group), 1000 mg/kg MCE (TIH+MCE1000 group), and 200 mg/kg fenofibrate (TIH+Fenofibrate group), respectively. Throughout the experiment, body weights and food intake were monitored, and the percentage reduction in body weight (BW) was calculated as 100 − (final BW − initial BW)/100. The feed efficiency ratio was determined by dividing the body weight gain (final BW − initial BW) by the mass of feed intake (total feed − remaining feed). Upon completion of the study, following a 12-h fasting period, animals from each group were anesthetized with light ether and euthanized. Various tissues, including fat, liver, kidney, and spleen samples were collected, along with blood, for biochemical and tissue analyses. Serum was extracted from 2 mL of whole blood collected in test tubes, which was subsequently centrifuged for 15 min at 3500 rpm. The serum samples were then stored at –70°C for further experimentation. Protein levels were quantified using the bicinchoninic acid (BCA) assay, with bovine serum albumin serving as the standard.

2.12 | Tissue analysis and histology

Following an overnight fasting period, tissues including liver, kidney, spleen, and epididymal fats were collected, weighed, and subsequently stored at –70°C as previously described (Choi et al., 2020). Additionally, the liver underwent perfusion with 10% formalin and was fixed for 24 h in 10% formalin before analysis. Histological assessment of fat accumulation in the frozen tissue was conducted using Oil Red O staining, with color intensity evaluated using ImageJ and expressed as a percentage (Choi et al., 2020). Liver samples were examined using a VENTANA DP600 slide scanner (Roche Diagnostics).

The frozen tissue was processed using a cryostat, fixed, and then stained with Oil Red O.

2.13 | Biochemical analysis

The serum concentrations of adiponectin and insulin were determined using ELISA assays (Sigma-Aldrich). The value of homeostasis model assessment of insulin resistance (HOMA-IR) was expressed as (fasting serum insulin × fasting serum glucose)/22.5 (Choi, Kim, Park, et al., 2023). Furthermore, the concentrations of various biomarkers in serum, such as total protein (TP), glucose, alanine aminotransferase (ALT) and aspartate aminotransferase (AST), HDL cholesterol, glucose, total cholesterol (TC), and triacylglycerol (TG) were analyzed using a Vitros 250 chemistry system from Ortho Clinical Diagnostics (Ortho Clinical Diagnostics). The levels of LDL and very LDL (VLDL) were calculated using Friedewald's formula (Kim et al., 2021), where LDL = TC − (HDL − TG/5) and VLDL = TG/5. Additionally, the atherogenic index (AI), cardiac risk ratio (CRR), atherogenic coefficient (AC), and coronary artery index (CAI) were evaluated using the equations established by Ikewuchi & Ikewuchi (Ikewuchi & Ikewuchi, 2009).

2.14 | Statistical analysis

The statistics of this study were conducted using the previous method (Choi et al., 2020; Choi, Park, et al., 2023), employing SPSS 21 (SPSS Inc.). The data obtained and examined from the present study were expressed as mean ± standard deviation (SD). To assess the statistical significance of comparisons between multiple groups, we performed a post hoc Tukey's test by utilizing one-way analysis of variance. Statistical significance was expressed as p values less than 0.05.

3 | RESULTS

3.1 | Effect of MCE and palmitic acid on cell viability in HepG2 cells

The effect of MCE on cell viability was assessed using the MTT assay on the HepG2 cell line. Various concentrations of MCE ranging from 50, 100, 300, 500, 700, 1000, 1500, and 2000 μg/mL were applied to the cell line, along with palmitic acid concentrations ranging from 50, 100, 300, 500, 700, 900, and 1000 μM, for a duration of 24 h. While treatment with MCE at concentrations up to 2000 μg/mL did not influence cell viability (Figure 1A), exposure to palmitic acid resulted in a significant decrease in cell viability at concentrations between 500 ($p < 0.05$), 700 ($p < 0.01$), 900 ($p < 0.01$), 1000 μM ($p < 0.01$) (Figure 1B).

3.2 | Effect of MCE on HMGCR activity in HepG2 cells

Following the evaluation of intracellular HMGCR activity, it was noted that treatment with MCE at concentrations of 50–300 μg/mL led to significant inhibition ($p < 0.01$) in a dose-dependent pattern of HMGCR activity (Figure 1C) compared to the group treated solely with palmitic acid. Additionally, a significant decrease ($p < 0.01$) of HMGCR activity was observed with atorvastatin treatment at concentrations of 100 μM compared to the group treated solely with palmitic acid.

3.3 | MCE contains D-pinitol compound

We found that MCE contains D-pinitol compound, and the concentrations detected in MCE were 12.01 mg/g at the peak compared to standard (Supporting Information S1: Figure S1), and further investigated in silico molecular docking property of MCE-derived D-pinitol on HMGCR, a therapeutic target for hyperlipidemia.

3.4 | In silico molecular docking on HMGCR

The molecular docking models of the ligands and enzymes are presented using Discovery Studio Visualizer software. Figure 1D,F displays the binding pockets of all ligands. D-pinitol interacts with 9 amino acids located in the cytosolic domain (residues 460–888) in which the active site of HMGCR, among which the amino acids of ALA753, ALA754, ASN755, ILE756, VAL757, THR758, TYR761, ASN771, and SER775, ASN755 and ILE756 form van der Waals interactions, a conventional hydrogen bond with ALA753, ALA754, THR758, ASN771, and SER775, unfavorable steric bumps interactions with ALA753, ALA754, ASN755, VAL757, THR758, ASN771, and SER775, and Pi-Cation of electrostatic interaction bonds with TYR761 by in Figure 1E and Table 2. Atorvastatin interacted with ALA754, ILE756, ALA769, and GLY773 by forming van der Waals, ALA753, THR758, ALA768, ASN771, and SER775 by conventional hydrogen bond, ALA768 by carbon hydrogen bond, VAL757, THR758, ALA768, ALA769, ASN771, and VAL772 by forming unfavorable steric bumps, ALA769, GLN770, and ASN771 by halogen (fluorine) of unfavorable interaction, and ILE762 by Alkyl of hydrophobic interaction in Figure 1F and Table 2. These docking results indicate that MCE-derived D-pinitol binds to the cytosolic domain as an active site of HMGCR, and several amino acids including ALA753, ALA754, ILE756, VAL757, THR758, ASN771, and SER775 matched the binding site of atorvastatin.

In the binding modes ($n = 10$) analyzed by Autodock Vina for HMGCR, MCE-derived D-pinitol exhibited the

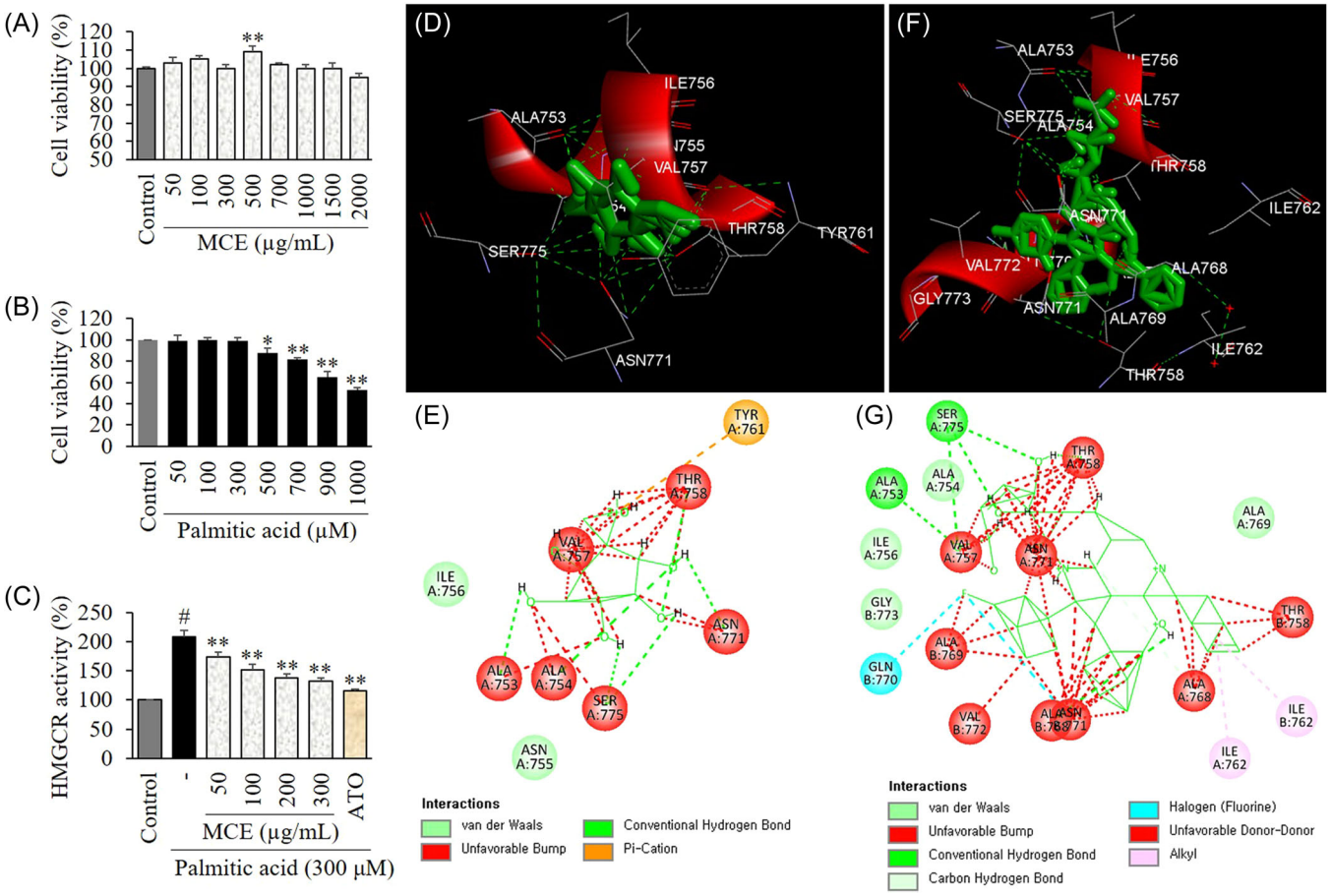


FIGURE 1 Effect of *Mesembryanthemum crystallinum* extract (MCE) on cell viability of MCE (A) or palmitic acid (B), 3-hydroxy-3-methylglutaryl-CoA reductase (HMGCR) activity in HepG2 cells (C), and 3D docking model (D) and interactions (E) of D-pinitol and 3D docking model (F) and interactions (G) of ATO on HMGCR. MTT assay showing the effect of MCE and palmitic acid on HepG2 cells viability. Cells were incubated with MCE at different concentrations (0–2000 μg/mL) or palmitic acid (0–1000 μM) for 24 h and cell viability was analyzed by MTT reduction assay. Each value is the mean ± SD of triplicate measurements. $*p < 0.05$ and $**p < 0.01$, compared with nontreated control group (A, B). $^{\#}p < 0.01$, compared with Control group, $**p < 0.01$, compared with palmitic acid only-treated group (C). ATO, atorvastatin.

average binding affinities were –8.53 kcal/mol (D-pinitol), and –8.21 kcal/mol (atorvastatin). The maximum binding affinities of –8.8 kcal/mol, and –8.9 kcal/mol in the same order, as shown in Table 3.

3.5 | Evaluation of toxicity predictions using the ProTox 3.0

We performed in silico analysis of the toxicity of the compounds of D-pinitol and atorvastatin, and Supporting Information S1: Table S1 displays the ProToxII findings. The LD_{50} of D-pinitol was estimated to be 804 mg/kg, and the LD_{50} was a predictive toxicity class of 4 (Supporting Information S1: Figure S2). We find some cases of toxicity, including nephrontoxicity, cardiotoxicity, and toxicity end points by BBB-barrier for D-pinitol (Supporting Information S1: Figures S3 and S4), whereas there was no toxicity on the skin in Pred-Skin outcome (Supporting Information S1: Figure S5). The result of toxicity prediction for atorvastatin shows it has a high probability of toxicity in 8 subjects and skin toxicity (Supporting Information S1: Figures S6–S9).

3.6 | Effect of MCE on body weight gain and feed efficiency in TIH mice model

Mice were injected with tyloxapol to induce a temporary hyperlipidemia of TIH model compared with MCE-administrated TIH group or nontreated control group fed a standard diet for 50 days. There were no significant differences on average body weight (Figure 2A), feed intake (Figure 2B), or BW increase rate (Figure 2C) among the MCE500, MCE1000, and Fenofibrate groups compared to the model group, excepting the result of feed efficiency rate in the model or Fenofibrate groups (Figure 2D).

TABLE 2 Molecular interaction of HMG-CoA reductase with MCE-derived D-pinitol and atorvastatin.

Ligand	Van der Waals	Hydrogen bond	Unfavorable	Electrostatic	Hydrophobic
D-pinitol	ASN755, ILE756*	Conventional: ALA753,* ALA754,* THR758,* ASN771,* SER775*	Steric bumps: ALA753,* ALA754,* VAL757,* THR758,* ASN771,* SER775*	Pi-Cation: TYR761	-
Atorvastatin	ALA754, ILE756, ALA769, GLY773	Conventional: ALA753, THR758, ALA768, ASN771, SER775 Carbon hydrogen: ALA768	Steric bumps: VAL757, THR758, ALA768, ALA769, ASN771, VAL772 Halogen (Fluorine): ALA769, GLN770, ASN771	-	Alkyl: ILE762

*Residues matching the binding site of atorvastatin. (-) interaction, not detected.

TABLE 3 Docking energy for the molecular binding of MCE-derived D-pinitol and atorvastatin on HMG-CoA reductase.

Ligand	Lowest binding energy (kcal/mol)	Average docking energy (kcal/mol)
D-pinitol	−8.8	−8.53 ($n = 10$)
Atorvastatin	−8.9	−8.21 ($n = 10$)

Note: Docking energy was analyzed by Autodock Vina. n = numbers of binding modes.

3.7 | Effect of MCE on the weight of tissues in TIH mice model

Table 4 presents the assessment of MCE and fenofibrate effects on the weight of different tissues from TIH model. The average weight of the liver was increased, whereas kidney and spleen weights were decreased on average in the model group compared to the control group. However, there were no significant alterations in their weight. MCE administration resulted in reduced liver weight gain, while the MCE-administered groups exhibited no significant change compared to the model group.

3.8 | Effect of MCE on hepatic and epididymal fats in TIH mice model

The weight of epididymal fat was lower on average in the model group compared to the control group, whereas there were no significant alterations in MCE-administered groups compared to the model group (Table 4). Additionally, we conducted a study to investigate the effect of MCE or fenofibrate administration on liver fat accumulation. Our analysis specifically examined hepatic fat density across different groups. As shown in Figure 3A,B, the injection of tyloxapol led to an increase (165%) in hepatic fat accumulation compared to the control group (100%). However, administration of MCE (Figure 3D,E) or fenofibrate (Figure 3C) resulted in a significant reduction (128% and 111%, or 134%) in fat accumulation and density by 57%–83% or 48%, compared to the model group (Figure 3F).

3.9 | Effect of MCE on serum biochemical parameters

Tyloxapol-induced hyperlipidemia is known to have close associations with adipokines, lipids, atherogenesis, cardiac risk, and insulin. Table 5 displays the serum levels of key biochemical parameters, encompassing proteins, glucose, insulin, lipids, adiponectin, and various indices. In comparison to the Control group, the TIH model group mice injected with tyloxapol resulted in elevated the levels of TC, TG, LDL, VLDL, AST, ALT, and atherogenic or cardiovascular-related parameters, except for adiponectin, which exhibited a significant decrease, and significant differences were not observed in TP, glucose, insulin, and insulin resistance values. MCE administration decreased the values of lipid metabolic parameters such as TC, TG, LDL, VLDL, ALT, and AST, while elevating the mean value of adiponectin and HDL. The Fenofibrate group exhibited significant reductions in insulin resistance, TC, TG, LDL, and VLDL levels, and a significant decrease in AST and ALT. The AI, AC, CRR, and CAI values were increased following tyloxapol injection compared to the Control group, as illustrated in Table 5. The increased values of AI, AC, CRR, and CAI were notably reduced in the MCE and Fenofibrate groups compared to the Model group.

4 | DISCUSSION

Dyslipidemia is closely linked to the levels of LDL and HDL and is known to contribute to several cardiovascular conditions, including arteriosclerosis, cardiovascular disease, and obesity. LDL is responsible for transporting cholesterol from the liver to peripheral tissues and cells (Choi et al., 2020; Choi, Kim, Park, et al., 2023). When oxidized, it is absorbed by scavenger receptors on macrophages, leading to the formation of foam cells. These foam cells contribute to the development of atherosclerotic plaques, thereby elevating the risk of cardiovascular disease (Stewart et al., 2020). The liver is crucial for maintaining cholesterol balance in our body. Cholesterol absorbed

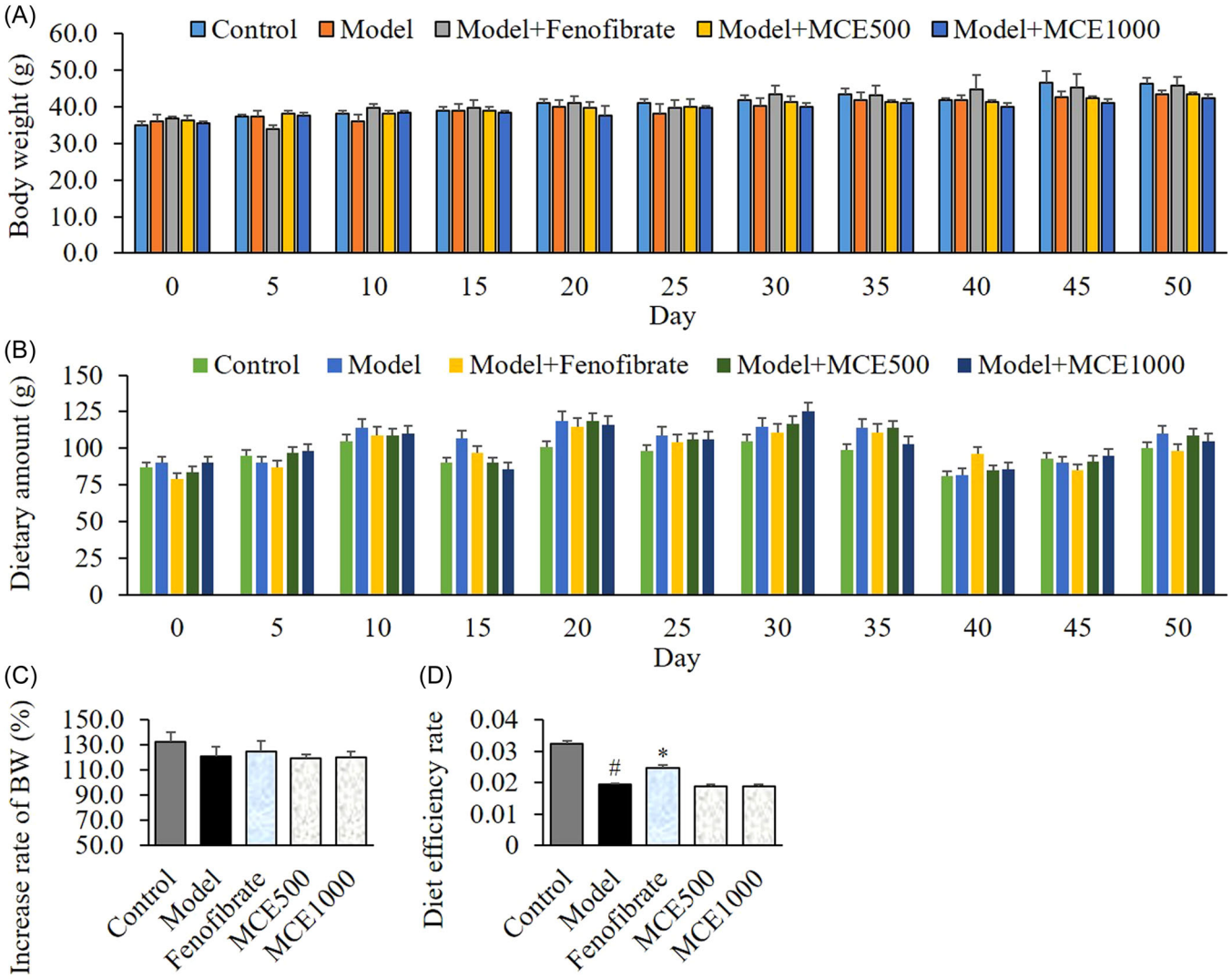


FIGURE 2 Effect of *Mesembryanthemum crystallinum* extract (MCE) on body weight (A), dietary amount (B), increase rate of BW (C), and diet efficiency rate (D) of TIH model. Each value is the mean ± SD ($n = 6$). $^{\#}p < 0.01$, compared with Control group, $^{*}p < 0.01$, compared with tyloxapol-induced hyperlipidemia (TIH) model group. Control, nontreated normal group; Model, TIH mice model group; Fenofibrate, 200 mg/kg fenofibrate-administrated TIH group, MCE500-1000, 500–1000 mg/kg MCE-administrated TIH group.

TABLE 4 Effect of MCE and fenofibrate on several tissues, and epididymal fat weights in tyloxapol-induced hyperlipedemic mice model.

Parameters	Control	Model	Fenofibrate	MCE500	MCE1000
Liver (g)	2.43 ± 0.12	2.57 ± 0.18	2.41 ± 0.24	2.50 ± 0.17	2.18 ± 0.07
Kidney (g)	0.89 ± 0.05	0.83 ± 0.03	0.83 ± 0.03	0.81 ± 0.06	0.84 ± 0.04
Spleen (g)	0.12 ± 0.01	0.11 ± 0.01	0.12 ± 0.02	0.12 ± 0.02	0.12 ± 0.01
Epididymal fat (g)	1.23 ± 0.10	0.99 ± 0.13	1.04 ± 0.20	1.05 ± 0.21	0.83 ± 0.09

Note: The data are presented as means ± SD, $n = 6$. One-way ANOVA followed by the post hoc Tukey test. Fenofibrate, 200 mg/kg/day fenofibrate-administrated model group; MCE500-1000, 500 and 1000 mg/kg/day *Mesembryanthemum crystallinum* extract-administrated model group.

from food, synthesized in other tissues, and produced within the liver itself all enter the liver's cholesterol pool. This cholesterol is then eliminated via the gallbladder as unmodified cholesterol, secreted into the small intestine as bile salts, or stored in peripheral tissues (Champe et al., 2005). Additionally, it is used as a component of plasma lipoproteins to regulate the intake and release of cholesterol (Champe et al., 2005). Cholesterol homeostasis is regulated not only by internal factors such as endocrine factors, body weight, circadian rhythm, and genetics but

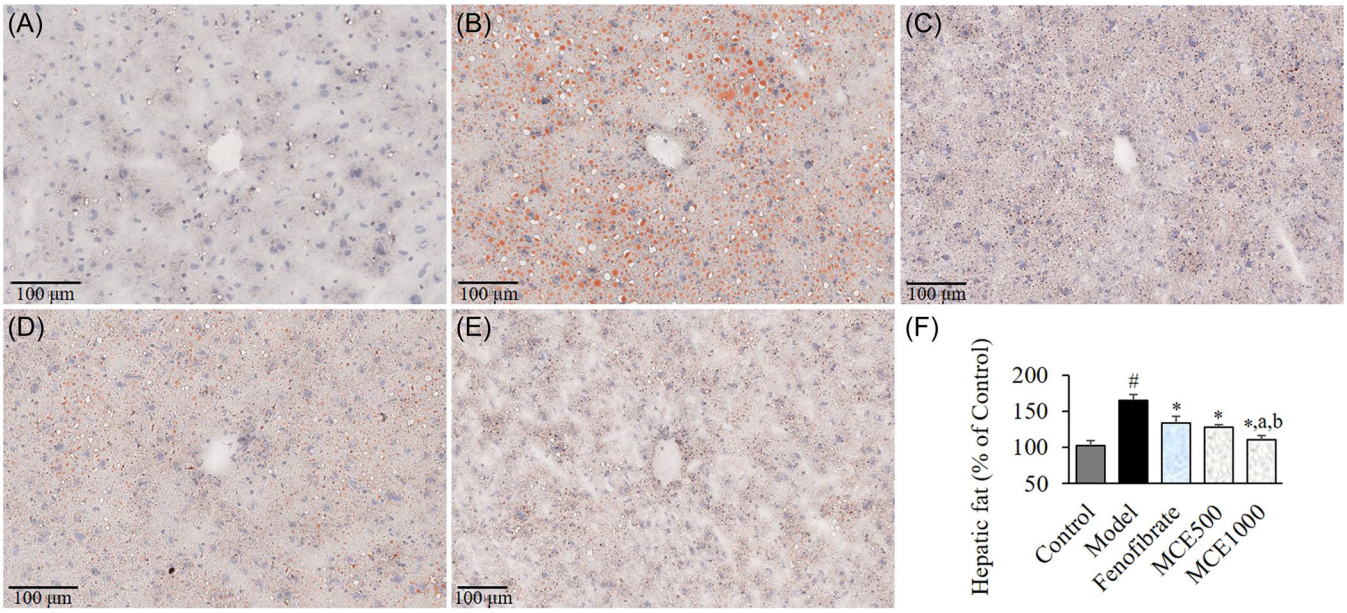


FIGURE 3 Histopathological analysis of hepatic fats from tyloxapol-induced hyperlipidemia (TIH) model. Effects of *Mesembryanthemum crystallinum* extract (MCE) and fenofibrate on hepatic fats in the TIH model were analyzed with H&E, microscope, and ImageJ. Each value is the mean ± SD ($n = 6$). $^{\#}p < 0.01$, compared with Control group, $^{*}p < 0.05$, compared with TIH model group. $^{a}p < 0.01$, compared with Fenofibrate group, $^{b}p < 0.05$, compared with MCE500 group. Control, nontreated normal group (A); Model, TIH mice model group (B); Fenofibrate, 200 mg/kg fenofibrate-administrated TIH group (C), MCE500-1000, 500 (D)-1000 mg/kg (E) MCE-extract-administrated TIH group. The color intensity of hepatic fat accumulation was evaluated using ImageJ and expressed as a percentage (F).

TABLE 5 Effects of MCE and fenofibrate on serum metabolic parameters from tyloxapol-induced hyperlipedemic mice model.

Parameters	Control	Model	Fenofibrate	MCE500	MCE1000
TP (mg/dL)	5.3 ± 0.5	5.3 ± 0.4	5.2 ± 0.3	5.3 ± 0.3	5.3 ± 0.5
Glucose (mg/dL)	160 ± 15	158 ± 11	154 ± 14	175 ± 9	173 ± 8
Insulin (μIU/mL)	5.76 ± 0.81	5.33 ± 0.72	4.90 ± 0.72	5.76 ± 0.62	5.65 ± 0.43
HOMA-IR	2.30 ± 0.16	2.08 ± 0.15	1.86 ± 0.13$^{\#}$	2.49 ± 0.17	2.41 ± 0.17
TC (mg/dL)	105 ± 8	257 ± 15$^{\#}$	117 ± 8**	192 ± 11**	171 ± 10**
TG (mg/dL)	91 ± 3	545 ± 11$^{\#}$	155 ± 9**	312 ± 15**	276 ± 12**
HDL (mg/dL)	102 ± 3	149 ± 1$^{\#}$	132 ± 9$^{\#}$	147 ± 2$^{\#}$	149 ± 1$^{\#}$
LDL (mg/dL)	21.2 ± 5.6	217.0 ± 16.2$^{\#}$	16.0 ± 0.8**	107.4 ± 12.0**	77.2 ± 11.4**
VLDL (mg/dL)	18.2 ± 0.6	109.0 ± 2.2$^{\#}$	31.0 ± 1.8**	62.4 ± 3.0**	55.2 ± 2.4**
AI	0.89 ± 0.03	3.66 ± 0.11$^{\#}$	1.17 ± 0.04**	2.12 ± 0.06**	1.85 ± 0.06**
AC	0.030 ± 0.001	1.00 ± 0.03$^{\#}$	-0.139 ± -0.004**	0.42 ± 0.01**	0.200 ± 0.006**
CRR	1.03 ± 0.03	1.72 ± 0.05$^{\#}$	0.89 ± 0.03**	1.31 ± 0.04**	1.15 ± 0.03**
CAI	0.21 ± 0.01	1.46 ± 0.04$^{\#}$	0.120 ± 0.004**	0.73 ± 0.02**	0.52 ± 0.02**
AST (U/L)	107.0 ± 2.4	182.4 ± 10.2$^{\#}$	135.5 ± 16.9*	146.1 ± 19.4*	142.4 ± 11.5*
ALT (U/L)	31.3 ± 1.1	47.5 ± 3.9$^{\#}$	34.5 ± 4.1*	43.9 ± 3.7	41.1 ± 3.5
Adiponectin (μg/mL)	6.01 ± 0.16	5.15 ± 0.09$^{\#}$	5.31 ± 0.15	5.32 ± 0.11	5.44 ± 0.13

Note: The data are presented as means ± SD, $n = 6$. One-way ANOVA followed by the post hoc Tukey test. $^{\#}p < 0.01$, compared to Control group. $^{*}p < 0.05$ and $^{**}p < 0.01$, compared to Model group. Fenofibrate, 200 mg/kg/day fenofibrate-administrated model group; MCE500-1000, 500, and 1000 mg/kg/day *Mesembryanthemum crystallinum* extract (MCE)-administrated model group; TP, total protein (mg/dL); Glucose (mg/dL); insulin (μIU/mL); HOMA-IR, homeostasis model assessment-insulin resistance; TC, total cholesterol (mg/dL); TG, triacylglycerol (mg/dL); HDL, high-density lipoprotein cholesterol (mg/dL); LDL, low-density lipoprotein cholesterol (mg/dL); VLDL, very low-density lipoprotein cholesterol (mg/dL); AI, atherogenic index; AC, atherogenic coefficient; CRR, cardiac risk ratio; CAI, coronary artery index; AST, aspartate aminotransferase (U/L); ALT, alanine aminotransferase (U/L); Adiponectin (μg/mL).

also by external nutritional and therapeutic factors like weight loss, statins, plant sterol therapy, and ezetimibe (Duan et al., 2022). Because the LDL reduction effect through diet and exercise is limited to 10%–15% (Scirica & Cannon, 2005), drug treatments have been employed to achieve more substantial outcomes, including statin therapy and non-statin alternatives. Medications used to treat dyslipidemia include statins, ezetimibe, and proprotein convertase subtilisin/kexin type 9 (PCSK9) inhibitors like alirocumab and evolocumab. Statins are the primary recommended treatment for dyslipidemia (Lee, 2015). They function as HMGCR inhibitors. HMGCR plays a role in cholesterol synthesis by converting HMG-CoA into mevalonic acid in the liver. Statins competitively inhibit HMGCR, thereby decreasing cholesterol production. Statins competitively inhibit HMGCR, thereby reducing cholesterol production (Jiang et al., 2018). However, numerous adverse reactions to statin drugs have been reported clinically and confirmed through various randomized controlled trials (Golomb & Evans, 2008; Pedersen & Tobert, 2004). Approximately 10%–15% of patients taking statins experience side effects such as muscle pain, besides common side effects like muscle pain and gastrointestinal symptoms, rarer symptoms such as rash, myopathy, and insomnia may also occur (Banach et al., 2015; Rosenson et al., 2017). In severe cases, muscle toxicity like rhabdomyolysis can develop (Choi & Park, 2004). Therefore, research on new drug materials that have cholesterol-controlling effects while alleviating the side effects of statins is continuing (Choi et al., 2020; Choi, Kim, Park, et al., 2023; Melia et al., 2023; Mozaffarian et al., 2022; Zhu et al., 2021). In the present study, we analyzed the levels of D-pinitol as a HMGCR inhibitor in MCE. D-pinitol, also referred to as 3-O-methyl-chiro-inositol, is a notable phytoconstituent (Abo-Elghiet et al., 2023) that displays insulin-like effects and protects pancreatic tissue from free radicals. Additionally, it exhibits anti-inflammatory, antihyperlipidemic, and hepatoprotective properties (Anandakumar et al., 2018). D-pinitol has long been recognized as a major component of soybean, with typical concentrations in soybean ranging from 1.3% to 2% (13–20 mg/g) of dry weight (Chen et al., 2014; Streeter, 2001). Comparing the results of D-pinitol contents in other study (Kim et al., 2005), the level (12.01 mg/g) of D-pinitol detected from MCE was higher than those of soybean (4.4–6.8 mg/g), soybean leaf (8.3 mg/g), defatted soybean (6.5 mg/g), ginseng (1.0–4.8 mg/g), and pine needle (7.0 mg/g), and lower than those of carob pod (40 mg/g), soy whey (20 mg/g), soybean oligosaccharides (17.4 mg/g, and *Boughainvillea* (20 mg/g).

Tyloxapol holds significant value in studies concerning triglyceride and cholesterol metabolism, serving as a crucial tool in animal models to assess lipid-lowering natural or chemical compounds and investigate cholesterol and triglyceride metabolism (Takahashi et al., 2003). This compound promotes cholesterol synthesis by enhancing the activity of HMGCR and subsequently elevates plasma cholesterol levels (Iqbal et al., 2015). Cholesterol control targeting HMGCR can be applied as an effective strategy, and studies are currently being actively reported on the search for HMGCR inhibitors and efficacy analysis from natural products and bioactive substances (Hahn et al., 2020; Ibrahim et al., 2020; Marahatha et al., 2021; Silva et al., 2021; Su et al., 2024). HMGCR catalyzes the conversion of HMG-CoA into mevalonic acid. Consequently, decreased HMGCR activity leads to reduced cellular cholesterol levels, triggering the activation of SREBP-mediated signaling pathways. HMGCR Class I features a transmembrane domain spanning residues 1 to 339, a cytosolic domain housing the active site in residues 460–888, and is linked by a region comprised of residues 340–459 (Friesen & Rodwell, 2004). The core active site responsible for reducing HMG-CoA is situated in the cis-loop, with key catalytic residues including GLU559, LYS691, LYS735, ASP767, and HIS866 (Miziorko, 2011). The CoA binding site is located in the L-domain of one monomer. The ADP moiety of CoA binds close to the enzyme's surface, within a pocket lined with positively charged residues (Gesto et al., 2020). The residues constituting the CoA binding pocket include SER565, ASN567, ARG568, LYS722, SER865, HIS866, and TYR479. NADPH binds to the S-domain of the adjacent subunit where the HMG-CoA binding pocket is situated. Residues SER626, ARG627, PHE628, ASP653, MET655, GLY656, MET657, ASN658, and VAL805 are derived from the S-domain, while residues ASN870 and ARG871 originate from the adjacent monomer. When NADPH is present, a conformational change occurs in the enzyme's C-terminus, resulting in the closure of the active site (Istvan, 2000). Statins possess rigid hydrophobic groups that are covalently attached to the HMG-like moiety. Specifically, atorvastatin, as a HMGCR inhibitor, establishes a hydrogen bond with a carbonyl oxygen atom at SER565, residing within a shallow groove between helices Lα1 and Lα10 with several residues including HIS752 and ASN755 (Istvan & Deisenhofer, 2001). In the present study, atorvastatin exhibited a docking energy of −8.21 kcal/mol and interacted with 13 amino acids (ALA753, ALA754, ILE756, VAL757, THR758, ILE762, ALA768, ALA769, GLN770, ASN771, VAL772, GLY773, and SER775) situated within the catalytic site of HMGCR. These interactions involved van der Waals forces, hydrogen bonds, unfavorable steric clashes, unfavorable halogen (fluorine) interactions, and hydrophobic alkyl interactions. MCE-derived D-pinitol exhibited the docking energy of −8.53 kcal/mol, respectively. They may influence enzymatic activity by forming strong affinity through van der Waals bonds (ILE756), conventional hydrogen bond interactions (ALA753, ALA754, THR758, ASN771, SER775), and unfavorable steric bumps bonds (ALA753, ALA754, VAL757, THR758, ASN771, SER775), which correspond to the binding site of atorvastatin. Notably, the binding affinities (kcal/mol) of D-pinitol to the active site of HMGCR were found to be higher than those of

atorvastatin. The strong docking ability of D-pinitol to interact with HMGCR influences its enzymatic activity. By ultimately reducing HMGCR activity, MCE-derived D-pinitol is expected to help control cholesterol production and metabolism, potentially alleviating the side effects associated with statin use in clinical practice. Moreover, tyloxapol treatment resulted in changes such as hypercholesterolemia, hyperlipidemia, increased LDL and VLDL levels, elevated AI, and hepatic fat accumulation in the TIH model, consistent with previous research findings (Mokhtari et al., 2023; Ramos et al., 2021; Sulumer et al., 2024). Compared to mice on a normal diet, those treated with tyloxapol exhibited a 1.65-fold increase in hepatic fat accumulation, which may be linked to cardiovascular risk. Furthermore, tyloxapol treatment resulted in elevated levels of TC, TG, LDL, VLDL, and cardiovascular risk indicators such as AI, AC, CRR, and CAI. Additionally, tyloxapol caused an increase in AST and ALT levels and a decrease in adiponectin levels in the serum of the TIH mouse model. However, administering MCE proved effective in lowering TC, TG, LDL, VLDL, AI, AC, CRR, CAI, and AST levels, and it demonstrated greater efficacy in increasing HDL levels compared to the Fenofibrate group. The beneficial effects of MCE may be attributed to the presence of inositol derivatives such as D-pinitol (Anderson et al., 1952), as well as beneficial compounds like β-carotene (Kang & Joo, 2023) and ferulic acid (Sun et al., 2022), which are known for their anti-inflammatory, antidiabetic, anti-LDL oxidation, and antioxidant properties.

5 | CONCLUSION

The effectiveness of MCE was evaluated in lowering fat/lipid/cholesterol levels. The result of HPLC analysis showed MCE contains D-pinitol compound (12.01 mg/g), and the docking simulations indicate MCE-derived D-pinitol binds to the cytosolic domain as an active site of HMGCR. In animal studies, there were no significant differences in body weight, feed intake, weights of epididymal fat, liver, kidney, and spleen among the MCE500, MCE1000, and Fenofibrate groups compared to the model group, whereas MCE effectively mitigated tyloxapol-induced hepatic fat accumulation, and an increase of cholesterols levels. This was achieved through improvements in metabolic parameters, including total cholesterol, triacylglycerol, HDL cholesterol, LDL cholesterol, very LDL, AI, AC, CRR, CAI, and aspartate aminotransferase, ultimately ameliorating TIH and hypercholesterolemia. These beneficial results suggest that MCE may be a strong potential for the attenuation of hyperlipidemia-related diseases and cholesterol/lipid accumulation.

AUTHOR CONTRIBUTIONS

Jun-Hui Choi: Conceptualization; formal analysis; investigation; methodology; software; validation; visualization; writing—original draft; writing—review and editing. **Se-Eun Park**: Formal analysis; investigation; methodology; writing—review and editing. **Seung Kim**: Conceptualization; funding acquisition; project administration; validation.

ACKNOWLEDGMENTS

This study was conducted by a research fund from Gwangju University, Republic of Korea in 2024. This research was supported by the R&D Program (RS-2023-00224984) funded by the Ministry of SMEs and Startups (MSS), Republic of Korea, in 2024.

CONFLICT OF INTEREST STATEMENT

The authors declare no conflicts of interest.

DATA AVAILABILITY STATEMENT

The data that has been used is confidential.

ETHICS STATEMENT

The animal study was reviewed and approved by the Institutional Animal Care and Use Committee of Chosun University (CIACUC2023-S0032).

ORCID

Seung Kim http://orcid.org/0000-0001-6249-8156

REFERENCES

Abo-Elghiet, F., Ahmed, A. H., Aly, H. F., Younis, E. A., Rabeh, M. A., Alshehri, S. A., Alshahrani, K. S. A., & Mohamed, S. A. (2023). D-pinitol content and antioxidant and antidiabetic activities of five *Bougainvillea spectabilis* Willd. cultivars. *Pharmaceuticals*, *16*, 1008.

Agarie, S., Kawaguchi, A., Kodera, A., Sunagawa, H., Kojima, H., Nose, A., & Nakahara, T. (2009). Potential of the common ice plant, *Mesembryanthemum crystallinum* as a new high-functional food as evaluated by polyol accumulation. *Plant Production Science*, *12*, 37–46.

Anandakumar, P., Vanitha, M. K., Gizaw, M., & Dereje, G. (2018). A review on the diverse effects of D-Pinitol. *Advanced Journal of Pharmacie and Life Science Research*, *6*, 1–7.

Anderson, A. B., MacDonald, D. L., & Fischer, H. O. L. (1952). The structure of pinitol. *Journal of the American Chemical Society*, *74*, 1479–1480.

Banach, M., Rizzo, M., Toth, P. P., Farnier, M., Davidson, M. H., Al-Rasadi, K., Aronow, W. S., Athyros, V., Djuric, D. M., Ezhov, M. V., Greenfield, R. S., Hovingh, G. K., Kostner, K., Serban, C., Lighezan, D., Fras, Z., Moriarty, P. M., Muntner, P., Goudev, A., … Mikhailidis, D. P. (2015). Statin intolerance - an attempt at a unified definition. Position paper from an international lipid expert panel. *Expert Opinion on Drug Safety*, *14*, 935–955.

Banerjee, P., Kemmler, E., Dunkel, M., & Preissner, R. (2024). ProTox 3.0: A webserver for the prediction of toxicity of chemicals. *Nucleic Acids Research*, *52*, W513–W520.

Champe, P. C., Harvey, R. A., & Ferrier, D. R. (2005). *Lippincott's illustrated reviews: Biochemistry* (3th ed., pp. 217–239). Lippincott Williams & Wilkins.

Chen, J., Zhang, H., Chen, Y., Wu, T., Yu, W., & Dai, G. (2014). Optimization of D-pinitol extraction from vegetable soybean leaves and its potential application in control of cucumber powdery mildew. *Crop Protection*, *60*, 20–27.

Choi, H. J., & Park, J. N. (2004). Management of risk of statin therapy. *Journal of the Korean Academy of Family Medicine*, *25*, 713–720.

Choi, J. H., Kim, K. M., Park, S. E., Kim, M. K., & Kim, S. (2023a). Short-term effects of PJE administration on metabolic parameters in diet-induced obesity mice. *Foods*, *12*, 1675.

Choi, J. H., Kim, M. K., Yeo, S. H., & Kim, S. (2020). Short-term *Cudrania tricuspidata* fruit vinegar administration attenuates obesity in high-fat diet-fed mice by improving fat accumulation and metabolic parameters. *Scientific Reports*, *10*, 21102.

Choi, J. H., & Kim, S. (2018). Mechanisms of attenuation of clot formation and acute thromboembolism by syringic acid in mice. *Journal of Functional Foods*, *43*, 112–122.

Choi, J. H., Park, S. M., & Kim, S. (2023b). Investigation of potential cGMP-specific PDE V and aminopeptidase N inhibitors of *Allium ampeloprasum* L. and its bioactive components: Kinetic and molecular docking studies. *International Journal of Molecular Sciences*, *24*, 13319.

Cousin, S. P., Hügl, S. R., Wrede, C. E., Kajio, H., Myers, Jr., M. G., & Rhodes, C. J. (2001). Free fatty acid-induced inhibition of glucose and insulin-Like growth factor I-induced deoxyribonucleic acid synthesis in the pancreatic β-cell line INS-11. *Endocrinology*, *142*, 229–240.

Drira, R., Matsumoto, T., Agawa, M., & Sakamoto, K. (2016). Ice plant (*Mesembryanthemum crystallinum*) extract promotes lipolysis in mouse 3T3-L1 adipocytes through extracellular signal-regulated kinase activation. *Journal of Medicinal Food*, *19*, 274–280.

Duan, Y., Gong, K., Xu, S., Zhang, F., Meng, X., & Han, J. (2022). Regulation of cholesterol homeostasis in health and diseases: From mechanisms to targeted therapeutics. *Signal Transduction and Targeted Therapy*, *7*, 265.

Foster, S., & Hobbs, C. (2002). *A field guide to western medicinal plants and herbs*. Houghton Mifflin Harcourt.

Friesen, J. A., & Rodwell, V. W. (2004). The 3-hydroxy-3-methylglutaryl coenzyme-A (HMG-CoA) reductases. *Genome Biology*, *5*, 248.

Gesto, D. S., Pereira, C. M. S., Cerqueira, N. M. F. S., & Sousa, S. F. (2020). An atomic-level perspective of HMG-CoA-reductase: The target enzyme to treat hypercholesterolemia. *Molecules*, *25*, 3891.

Golomb, B. A., & Evans, M. A. (2008). Statin adverse effects: A review of the literature and evidence for a mitochondrial mechanism. *American Journal of Cardiovascular Drugs*, *8*, 373–418.

Guan, J. Z., Tamasawa, N., Murakami, H., Matsui, J., Tanabe, J., Matsuki, K., Yamashita, M., & Suda, T. (2008). HMG-CoA reductase inhibitor, simvastatin improves reverse cholesterol transport in type 2 diabetic patients with hyperlipidemia. *Journal of Atherosclerosis and Thrombosis*, *15*, 20–25.

Hahn, H. J., Abagyan, R., Podust, L. M., Roy, S., Ali, I. K. M., & Debnath, A. (2020). HMG-CoA reductase inhibitors as drug leads against *Naegleria fowleri*. *ACS Chemical Neuroscience*, *11*, 3089–3096.

Han, L., Lai, P., & Du, J. R. (2014). Deciphering molecular mechanism underlying hypolipidemic activity of echinocystic acid. *Evidence-Based Complementary and Alternative Medicine*, *2014*, 823154.

Hu, N., Chen, C., Wang, J., Huang, J., Yao, D., & Li, C. (2021). Atorvastatin ester regulates lipid metabolism in hyperlipidemia rats via the PPAR-signaling pathway and HMGCR expression in the liver. *International Journal of Molecular Sciences*, *22*, 11107.

Ibrahim, A., Shafie, N. H., Mohd Esa, N., Shafie, S. R., Bahari, H., & Abdullah, M. A. (2020). *Mikania micrantha* extract inhibits HMG-CoA reductase and ACAT2 and ameliorates hypercholesterolemia and lipid peroxidation in high cholesterol-fed rats. *Nutrients*, *12*, 3077.

Ibtissem, B., Abdelly, C., & Sfar, S. (2012). Antioxidant and atibacterial poperties of *Mesembryanthemum crystallinum* and *Carpobrotus edulis* extracts. *Advances in Chemical Engineering and Science*, *2*, 20828.

Ikewuchi, C. J., & Ikewuchi, C. C. (2009). Alteration of plasma lipid profiles and atherogenic indices by *Stachytarpheta jamaicensis* L. (Vahl). *Biokemistri*, *21*, 71–77.

Iqbal, D., Khan, M. S., Khan, M. S., Ahmad, S., Hussain, M. S., & Ali, M. (2015). Bioactivity guided fractionation and hypolipidemic property of a novel HMG-CoA reductase inhibitor from *Ficus virens* Ait. *Lipids in Health and Disease*, *14*, 15.

Istvan, E. (2000). The structure of the catalytic portion of human HMG-CoA reductase. *Biochimica et Biophysica Acta (BBA)-Molecular and Cell Biology of Lipids*, *1529*, 9–18.

Istvan, E. S., & Deisenhofer, J. (2001). Structural mechanism for statin inhibition of HMG-CoA reductase. *Science*, *292*, 1160–1164.

Jiang, S. Y., Li, H., Tang, J. J., Wang, J., Luo, J., Liu, B., Wang, J. K., Shi, X. J., Cui, H. W., Tang, J., Yang, F., Qi, W., Qiu, W. W., & Song, B. L. (2018). Discovery of a potent HMG-CoA reductase degrader that eliminates statin-induced reductase accumulation and lowers cholesterol. *Nature Communications*, *9*, 5138.

Kang, S., Kim, S., Ha, S., Lee, C., & Nam, S. (2016). Biochemical components and physiological activities of ice plant (*Mesembryanthemum crystallinum*). *Journal of the Korean Society of Food Science and Nutrition*, *45*, 1732–1739.

Kang, Y. W., & Joo, N. M. (2023). Comparative analysis on phytochemical properties, anti-oxidative, and anti-inflammatory activities of the different organs of the common ice plant *Mesembryanthemum crystallinum* L. *Applied Sciences*, *13*, 2527.

Kim, J. H., Seo, H. J., Pang, Q. Q., Kwon, Y. R., Kim, J. H., & Cho, E. J. (2021). Protective effects of krill oil on high fat diet-induced cognitive impairment by regulation of oxidative stress. *Free Radical Research*, *55*, 700–710.

Kim, J. I., Kim, J. C., Joo, H. J., Jung, S. H., & Kim, J. J. (2005). Determination of total chiro-inositol content in selected natural materials and evaluation of the antihyperglycemic effect of pinitol isolated from soybean and carob. *Food Science and Biotechnology*, *14*, 441–445.

Kim, K. J., Kang, N. E., Oh, Y. S., & Jang, S. E. (2023). Eupatilin alleviates hyperlipidemia in mice by inhibiting HMG-CoA reductase. *Biochemistry Research International*, *2023*, 1–5.

Kumai, T., Oonuma, S., Matsumoto, N., Takeba, Y., Taniguchi, R., Kamio, K., Miyazu, O., Koitabashi, Y., Sekine, S., Tadokoro, M., & Kobayashi, S. (2004). Anti-lipid deposition effect of HMG-CoA reductase inhibitor, pitavastatin, in a rat model of hypertension and hypercholesterolemia. *Life Sciences*, *74*, 2129–2142.

Lee, H. J., Park, S. E., & Kim, S. (2019). *Cudrania tricuspidata* fruit extract ameliorates free fatty acid-induced lipid accumulation in HepG2 cells. *Journal of Life Science*, *29*, 1144–1151.

Lee, S. H. (2015). Update on the pharmacologic agents for dyslipidemia. *The Journal of Korean Diabetes*, *16*, 269–275.

Lu, J., Meng, Z., Cheng, B., Liu, M., Tao, S., & Guan, S. (2019). Apigenin reduces the excessive accumulation of lipids induced by palmitic acid via the AMPK signaling pathway in HepG2 cells. *Experimental and Therapeutic Medicine*, *18*, 2965–2971.

Marahatha, R., Basnet, S., Bhattarai, B. R., Budhathoki, P., Aryal, B., Adhikari, B., Lamichhane, G., & Parajuli, N. (2021). Potential natural inhibitors of xanthine oxidase and HMG-CoA reductase in cholesterol regulation: In silico analysis. *BMC Complementary Medicine and Therapies*, *21*(1), 1.

Melia, S., Juliyarsi, I., Kurnia, Y., Aritonang, S., Purwati, E., Sukma, A., Fitria, N., Susmiati, S., Meinapuri, M., Pratama, Y., & Ramadhanti, N. (2023). Effect of fermented milk *Pediococcus acidilactici* BK01 on cholesterol and microbiota in Wistar mice intestine. *Journal of Advanced Veterinary and Animal Research*, *10*, 64–71.

Miziorko, H. M. (2011). Enzymes of the mevalonate pathway of isoprenoid biosynthesis. *Archives of Biochemistry and Biophysics*, *505*, 131–143.

Mokhtari, I., Mokhtari, C., Moumou, M., Harnafi, M., Milenkovic, D., Amrani, S., Hakmaoui, A., & Harnafi, H. (2023). Polyphenol-rich extract from loquat fruit peel prevents hyperlipidemia and hepato-nephrotoxicity in mice: In vivo study and in silico prediction of possible mechanisms involving identified polyphenols and/or their circulating metabolites. *Food & Function*, *14*, 7489–7505.

Morris, G. M., Huey, R., Lindstrom, W., Sanner, M. F., Belew, R. K., Goodsell, D. S., & Olson, A. J. (2009). AutoDock4 and AutoDockTools4: Automated docking with selective receptor flexibility. *Journal of Computational Chemistry*, *30*, 2785–2791.

Mozaffarian, D., Maki, K. C., Bays, H. E., Aguilera, F., Gould, G., Hegele, R. A., Moriarty, P. M., Robinson, J. G., Shi, P., Tur, J. F., Lapointe, J. F., Aziz, S., Lemieux, P., Hao, T., Mirza, L., Kipp, G., Jarrett, W., Little, R., Mariano, H., … Olvera Alvarez, I. (2022). Effectiveness of a novel ω-3 krill oil agent in patients with severe hypertriglyceridemia: A randomized clinical trial. *JAMA Network Open*, *5*, e2141898.

Olivier, P., Plancke, M. O., Marzin, D., Clavey, V., Sauzieres, J., & Fruchart, J. C. (1998). Effects of fenofibrate, gemfibrozil and nicotinic acid on plasma lipoprotein levels in normal and hyperlipidemic mice A proposed model for drug screening. *Atherosclerosis*, *70*(1–2), 107–114.

Palabıyık, E., Sulumer, A. N., Uguz, H., Avcı, B., Askın, S., Askın, H., & Demir, Y. (2023). Assessment of hypolipidemic and anti-inflammatory properties of walnut (*Juglans regia*) seed coat extract and modulates some metabolic enzymes activity in triton WR-1339-induced hyperlipidemia in rat kidney, liver, and heart. *Journal of Molecular Recognition*, *36*, e3004.

Pedersen, T. R., & Tobert, J. A. (2004). Simvastatin: A review. *Expert Opinion on Pharmacotherapy*, *5*, 2583–2596.

Ramos, L., Justino, A. B., Tavernelli, N., Saraiva, A. L., Franco, R. R., de Souza, A. V., Silva, H., de Moura, F., Botelho, F. V., & Espindola, F. S. (2021). Antioxidant compounds from *Annona crassiflora* fruit peel reduce lipid levels and oxidative damage and maintain the glutathione defense in hepatic tissue of Triton WR-1339-induced hyperlipidemic mice. *Biomedicine & Pharmacotherapy = Biomedecine & Pharmacotherapie*, *142*, 112049.

Rosenson, R. S., Baker, S., Banach, M., Borow, K. M., Braun, L. T., Bruckert, E., Brunham, L. R., Catapano, A. L., Elam, M. B., Mancini, G. B. J., Moriarty, P. M., Morris, P. B., Muntner, P., Ray, K. K., Stroes, E. S., Taylor, B. A., Taylor, V. H., Watts, G. F., & Thompson, P. D. (2017). Optimizing cholesterol treatment in patients with muscle complaints. *Journal of the American College of Cardiology*, *70*, 1290–1301.

Saxena, N., & Chandra, N. C. (2021). Cholesterol: A prelate in cell nucleus and its serendipity. *Current Molecular Medicine*, *20*, 692–707.

Schrodinger, L. L. C. (2010). The PyMOL Molecular Graphics System (Version 3.0.0).

Scirica, B. M., & Cannon, C. P. (2005). Treatment of elevated cholesterol. *Circulation*, *111*, e360–e363.

Silva, M., Philadelpho, B., Santos, J., Souza, V., Souza, C., Santiago, V., Silva, J., Souza, C., Azeredo, F., Castilho, M., Cilli, E., & Ferreira, E. (2021). IAF, QGF, and QDF peptides exhibit cholesterol-lowering activity through a statin-like HMG-CoA reductase regulation mechanism: In silico and in vitro approach. *International Journal of Molecular Sciences*, *22*, 11067.

Stewart, J., McCallin, T., Martinez, J., Chacko, S., & Yusuf, S. (2020). Hyperlipidemia. *Pediatrics in Review*, *41*, 393–402.

Streeter, J. G. (2001). Simple partial purification of d-pinitol from soybean leaves. *Crop Science*, *41*, 1985–1987.

Su, X. Z., Zhang, L. F., Hu, K., An, Y., Zhang, Q. P., Tang, J. W., Yan, B. C., Li, X. R., Cai, J., Li, X. N., Sun, H. D., Jiang, S. Y., & Puno, P. T. (2024). Discovery of natural potent HMG-CoA reductase degraders for lowering cholesterol. *Angewandte Chemie International Edition*, *63*, e202313859.

Sulumer, A. N., Palabıyık, E., Avcı, B., Uguz, H., Demir, Y., Serhat Özaslan, M., & Aşkın, H. (2024). Protective effect of bromelain on some metabolic enzyme activities in tyloxapol-induced hyperlipidemic rats. *Biotechnology and Applied Biochemistry*, *71*, 17–27.

Sun, M., Wei, Y., Feng, X., Fan, J., & Chen, X. (2022). Composition, anti-LDL oxidation, and non-enzymatic glycosylation inhibitory activities of the flavonoids from *Mesembryanthemum crystallinum*. *Frontiers in Nutrition*, *9*, 963858.

Takahashi, Y., Inaba, N., Kuwahara, S., & Kuki, W. (2003). Effects of γ-terpinene on lipid concentrations in serum using triton WR1339-treated rats. *Bioscience, Biotechnology, and Biochemistry*, *67*, 2448–2450.

Zhang, Y., Jia, X.-B., Liu, Y.-C., Yu, W.-Q., Si, Y.-H., & Guo, S.-D. (2022). Fenofibrate enhances lipid deposition via modulating PPARγ, SREBP-1c, and gut microbiota in ob/ob mice fed a high-fat diet. *Frontiers in Nutrition*, 9.

Zhang, C., Wu, W., Xin, X., Li, X., & Liu, D. (2019). Extract of ice plant (*Mesembryanthemum crystallinum*) ameliorates hyperglycemia and modulates the gut microbiota composition in type 2 diabetic Goto-Kakizaki rats. *Food & Function*, *10*, 3252–3261.

Zhu, L. Y., Wen, X. Y., Xiang, Q. Y., Guo, L. L., Xu, J., Zhao, S. P., & Liu, L. (2021). Comparison of the reductions in LDL-C and non-HDL-C induced by the red yeast rice extract Xuezhikang between fasting and non-fasting states in patients with coronary heart disease. *Frontiers in Cardiovascular Medicine*, *8*, 674446.

SUPPORTING INFORMATION

Additional supporting information can be found online in the Supporting Information section at the end of this article.

How to cite this article: Choi, J.-H., Park, S.-E., & Kim, S. (2024). Effect of *Mesembryanthemum crystallinum* and its derived D-pinitol on HMG-CoA reductase and tyloxapol-induced hyperlipedemia. *eFood*, *5*(6), e70020. https://doi.org/10.1002/efd2.70020